Quasilinear diffusion of protons by equatorial magnetosonic waves at quasi-perpendicular propagation: Comparison with the test-particle approach

Kyungguk Min[1], Kaijun Liu[2]

[1]Department of Astronomy and Space Science, Chungnam National University, Daejeon, Korea.
[2]Department of Earth and Space Sciences, Southern University of Science and Technology, Shenzhen, China.

Key Points:

- QL diffusion coefficients of protons scattered by MSWs at quasi-perpendicular propagation are verified
- Proton dynamics due to MSWs at perpendicular propagation are examined in detail using test-particle tracing
- Non-zero wave power at $\gtrsim 89.5^\circ$ WNAs typically excluded can be important for ring current proton dynamics

Corresponding author: Kyungguk Min, kyungguk@me.com

Abstract

Although some plasma waves exhibit the largest growth rate and amplitude at 90° wave normal angle (WNA), particle scattering by these waves in a quasilinear (QL) sense has not been examined previously. Using test-particle calculation and QL theory, the present study investigates the proton scattering by equatorial fast magnetosonic waves (MSWs; a.k.a equatorial noise) with varying WNAs including 90°. Comparison with the diffusion coefficients in momentum space obtained from the test-particle approach indicates that the QL diffusion coefficients given by, e.g., Kennel and Engelmann (1966) are valid up to 90° WNA, provided that MSWs described conform to the usual QL theory assumptions. The test-particle dynamics due to MSWs at 90° WNA are examined in detail. Although in the QL picture, protons are only supposed to resonate with MSWs of integer harmonic frequencies at perpendicular propagation, the presence of slightly off-integer harmonic modes as part of a narrowband discrete spectrum of incoherent MSWs plays an important role in making the proton scattering stochastic. Considering the recent test-particle result of bounce-averaged resonance of energetic protons, non-zero wave power at the WNAs $\gtrsim 89.5°$ typically excluded in QL diffusion can be important for ring current proton dynamics.

1 Introduction

Plasma waves in the inner magnetosphere play an important role in the dynamics of the radiation belts and ring current (e.g., Thorne, 2010). Gyro-resonant wave-particle interactions in the inner magnetosphere (and space plasmas in general) are typically described in terms of quasilinear (QL) theory (Kennel & Engelmann, 1966). According to this theory, the dynamics of particles are described by a Fokker-Planck-type diffusion equation (Schulz & Lanzerotti, 1974). The diffusion coefficients in this equation encapsulate the physics of wave-particle interactions in the QL limit. As diffusion simulations are the only practical way to model the long-term behavior of the radiation belts and ring current at present, calculation of the diffusion coefficients appropriate for the inner magnetosphere has been the focus of numerous studies (e.g., Lyons, 1974; Glauert & Horne, 2005; Summers, 2005; Albert, 2005, 2007; Mourenas et al., 2013).

The diffusion coefficients in QL theory depend on wave spectra and plasma properties. A standard—though not necessary—way to describe the wave spectra is to use truncated Gaussian distributions both in frequency and wave normal angle spaces (Lyons, 1974). Particularly, for wave spectra in wave normal angle space, the usual choice is $g_\omega(\psi) \propto \exp[-(\tan\psi - \tan\psi_m)^2 / \tan^2\Delta\psi]$, where ψ is the wave normal angle, and $\tan\psi_m$ and $\tan\Delta\psi$ determine the extent of the wave distribution. The effect of using $\tan\psi$ in the Gaussian model is to reduce the power ascribed to large values of ψ (Albert, 2007). That is, as ψ approaches 90°, $g_\omega(\psi)$ tends to zero regardless of the values of ψ_m and $\Delta\psi$ chosen. Furthermore, by virtue of the truncated Gaussian, g_ω is zero unless ψ lies between $\psi_{\min}$ and $\psi_{\max}$, where it is customary to assume $\psi_{\max} < 90°$. Diffusion simulations with the diffusion coefficients calculated as such for the major plasma waves in the inner magnetosphere have been widely used to understand the acceleration and loss processes of relativistic electrons in the radiation belts (e.g., Thorne et al., 2013; Ma et al., 2015; Drozdov et al., 2020).

While the above Gaussian model in wave normal angle may be appropriate to represent the spectra of waves at quasi-parallel and moderately oblique propagation (such as whistler-mode waves and electromagnetic ion cyclotron waves in the inner magnetosphere), it may not be an ideal choice to describe the waves whose maximum growth rate occurs at ψ close to or exactly at 90°. In the inner magnetosphere, the latter category includes equatorial fast magnetosonic waves (a.k.a equatorial noise; MSWs hereafter) which are driven by a proton ring distribution with the maximum growth rate occurring at $\psi =$ 90° (e.g., Horne et al., 2000) and at frequencies multiples of the proton cyclotron frequency.

Nevertheless, many previous studies adopted the truncated Gaussian distribution for the wave normal angle distribution of MSWs (e.g., Horne et al., 2007; Xiao et al., 2014, 2015; Ma et al., 2019). The typically used parameters are those from Horne et al. (2007), where $\psi_m = 89°$ and $\Delta\psi = 86°$ (or some variants thereof), which result in negligible wave energy above $\psi = 89.5°$. Other studies used a constant value less than 90° for the wave normal angle, say, $\psi = 89°$ (e.g., Ni et al., 2017). Neglecting MSWs at $\psi \gtrsim 89.5°$ is perhaps well justified for studying the scattering of radiation belt electrons because these electrons are primarily affected by Landau resonance (Horne et al., 2000, 2007) and the parallel component of the fluctuating electric field tends to zero at exact perpendicular propagation. For example, Lei et al. (2017) showed that MSWs with $\psi \lesssim 87°$ causes the most efficient electron scattering. In contrast, excluding the contribution from MSWs at quasi-perpendicular propagation (where both simulations and observations indicate the maximum power occurs (Boardsen et al., 2018; Min et al., 2020)) can potentially lead to an underestimation of the scattering of energetic ring current protons to which high-order cyclotron resonances play a dominant role (e.g., Fu et al., 2016; Fu & Ge, 2021). Particularly, Fu and Ge (2021) showed that, in their test-particle results, the proton heating induced by MSWs becomes relatively stable for $\psi \gtrsim 88°$. (They considered wave normal angles up to 89.9°.) This raises an important question of whether neglecting the contribution from MSWs at quasi-perpendicular propagation is well justified for the proton scattering.

In the present study, we investigate the transition of the scattering of protons interacting with low-amplitude, broadband, incoherent MSWs as ψ approaches 90° in a uniform background magnetic field. Such a scenario has been examined previously by Curtis (1985) who suggested that the perpendicular ion heating in the equatorial plasmasphere is the result of MSWs at quasi-perpendicular propagation. To calculate the perpendicular momentum diffusion coefficient, Curtis (1985) made several simplifying assumptions appropriate for the equatorial plasmasphere. In the present study, we relax some of their assumptions and additionally use the test-particle (TP) approach to verify and complement the results of QL diffusion theory. By comparing with the TP computation, we first show that the QL diffusion coefficients of Kennel and Engelmann (1966) remain valid at $\psi = 90°$. For simplicity of analysis, we assume broadband MSWs in wavenumber (or equivalently in frequency) with a fixed ψ at a time. We then investigate in detail the test particle dynamics due to MSWs at $\psi = 90°$, which are mainly governed by the electrostatic fluctuations.

The organization of the paper is as follows. In Section 2, we present QL and TP theoretical constructs and in Section 3 we use them to calculate the diffusion coefficients. Section 4 concludes the paper.

2 Theory

We consider a homogeneous, magnetized plasma in a uniform background magnetic field. We choose a coordinate system where the background magnetic field is along the z direction and the wave vector is contained in the $x-z$ plane. The formulation below assumes the use of the gauss unit system.

2.1 Diffusion Coefficients

According to Kennel and Engelmann (1966), the diffusion equation for some proton distribution, f, can be written as

$$\frac{\partial f}{\partial t} = \frac{1}{v_\perp}\frac{\partial}{\partial v_\perp}\left[v_\perp\left(D_{\perp\perp}\frac{\partial}{\partial v_\perp} + D_{\perp\parallel}\frac{\partial}{\partial v_\parallel}\right)\right]f + \frac{1}{v_\perp}\frac{\partial}{\partial v_\parallel}\left[v_\perp\left(D_{\parallel\perp}\frac{\partial}{\partial v_\perp} + D_{\parallel\parallel}\frac{\partial}{\partial v_\parallel}\right)\right]f, \tag{1}$$

where $D_{\mu\nu}$ are the diffusion coefficients in velocity space. The directional subscripts are, as usual, with respect to the background magnetic field, $\mathbf{B}_0$. Note that the dimension of $D_{\mu\nu}$ is velocity squared per time.

In this subsection, we simplify the diffusion coefficients given by Kennel and Engelmann (1966) appropriate for the problem we are considering here. We make several assumptions which are well justified for MSWs under consideration. First, we ignore the parallel component of the fluctuating electric field, $E_\parallel^w$. Unlike electrons which are magnetized and primarily affected by Landau resonance, protons are much heavier and slower, and thus less susceptible to Landau resonance. Furthermore, according to cold plasma dispersion theory, the ratio of $|E_\parallel^w|$ to the amplitude of the fluctuating electric field ($\mathbf{E}^w$) remains $|E_\parallel^w|/|\mathbf{E}^w| \lesssim 0.02$ for $\psi \geq 80^\circ$ and frequencies $\omega \lesssim 40\Omega_p$, where Ω_p is the proton (angular) cyclotron frequency. Throughout the paper, we assume MSWs with $\omega \lesssim 20\Omega_p$ and $\psi \geq 80^\circ$, in which case $|E_\parallel^w|/|\mathbf{E}^w| < 0.01$. Second, we consider broadband MSWs propagating in a single direction so that all constituent waves have the same wave normal angle, ψ. This is a commonly used approach in investigations involving TP computation (e.g., Fu et al., 2016) and simplifies the wave description in TP computation. Last, we assume that the growth rate (i.e., the imaginary part of the complex wave frequency) is negligible so that the integrable singularities in $D_{\mu\nu}$ can be replaced with the delta function.

After considering these conditions, we may reduce the diffusion coefficients in Kennel and Engelmann (1966) to

$$D_{\mu\nu} = \pi\,\Omega_p c^2 \sum_{n=-\infty}^{\infty} \sum_j \frac{|\mathcal{E}_n|^2}{B_0^2} \frac{\Delta_\mu^* \Delta_\nu}{|\partial\zeta_n/\partial k|}, \tag{2}$$

where the summation index n is the cyclotron resonance order and k is the wavenumber along the selected propagation direction (i.e., selected ψ). The definitions of $\zeta_n(k)$, $\mathcal{E}_n(k)$, $\Delta_\parallel(k)$, and $\Delta_\perp(k)$ are as follows:

$$\zeta_n(k) = \frac{k_\parallel v_\parallel - (\omega_\mathbf{k} - n\Omega_p)}{\Omega_p}; \tag{3}$$

$$\mathcal{E}_n(k) = \frac{\tilde{E}_\mathbf{k}^r J_{n+1}(\xi) + \tilde{E}_\mathbf{k}^l J_{n-1}(\xi)}{\sqrt{2}}; \tag{4}$$

$$\Delta_\perp(k) = 1 - \frac{k_\parallel v_\parallel}{\omega_\mathbf{k}}; \quad \text{and} \quad \Delta_\parallel(k) = \frac{k_\parallel v_\perp}{\omega_\mathbf{k}}. \tag{5}$$

Here, J_n is the Bessel function of the first kind with an argument, $\xi = k_\perp v_\perp/\Omega_p$. The summation over j in Eq. (2) should consider all resonant k_j's which are the solutions to the resonance condition, $\zeta_n(k) = 0$, for given ψ.

In general, ζ_n is also a function of $v_\parallel$. However, if $k_\parallel = 0$ (i.e., $\psi = 90^\circ$), ζ_n becomes independent of $v_\parallel$ and so does the resonance condition, $\omega_\mathbf{k} = n\Omega_p$. (Chen (2015) characterized this situation as being non-resonant.) As one can see, for $\varphi \equiv \psi - \pi/2 \sim 0$, it follows $\Delta_\perp \sim \mathcal{O}(1)$ and $\Delta_\parallel \sim \mathcal{O}(\varphi)$, and thus $D_{\parallel\parallel}/D_{\perp\perp} \sim \mathcal{O}(\varphi^2)$. Therefore, the proton diffusion by MSWs dominates in the velocity direction perpendicular to $\mathbf{B}_0$.

Information about the wave power spectral distribution is contained in $\tilde{E}_\mathbf{k}^r \equiv (\tilde{E}_\mathbf{k}^x - i\tilde{E}_\mathbf{k}^y)/\sqrt{2}$ and $\tilde{E}_\mathbf{k}^l \equiv (\tilde{E}_\mathbf{k}^x + i\tilde{E}_\mathbf{k}^y)/\sqrt{2}$ which represent the right-hand and left-hand polarized electric field fluctuations, respectively. The relationship among the electric and magnetic field wave components is readily available from cold plasma dispersion theory, e.g., J. Li et al. (2015, Eqs. (3a)–(3f)).

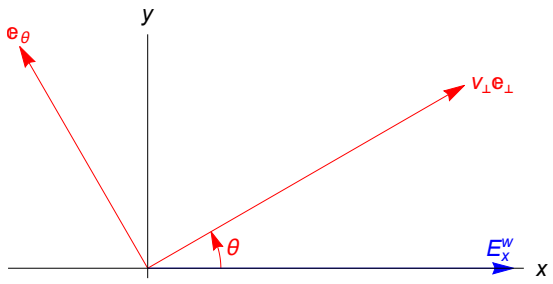

Figure 1. The relationship between the test particle's velocity vector direction, $\mathbf{e}_\perp$, and the x component of the fluctuating electric field, E_x^w. The angle θ denotes the gyro-phase angle of the particle. The unit vectors $\mathbf{e}_\perp$ and $\mathbf{e}_\theta$ orthogonal to each other are a function of θ.

2.2 Test-particle Tracing

Equations of motion of individual (non-relativistic) test protons are given by

$$\frac{d\mathbf{v}}{dt} = \frac{e}{m_p}\left(\mathbf{E}^w + \frac{\mathbf{v}}{c}\times\mathbf{B}\right), \tag{6}$$

where e is the elementary charge, m_p is the proton mass, and $\mathbf{v}$ is the particle velocity. Unless otherwise specified, all TP calculations shown here are done by solving this equation using the Boris method (Birdsall & Langdon, 2004), with all three components of the MSW electric and magnetic fields retained.

In order to interpret the dynamics of protons interacting with MSWs at $\psi = 90°$ in detail, in what follows we take the standard procedure typically used to simplify Eq. (6) further (e.g., J. Li et al., 2015; Fu et al., 2016). We start by defining a coordinate system shown in Figure 1, where $\mathbf{B}_0 = B_0\hat{z}$ and $\mathbf{k} = k_x\hat{x}$ (note that $\psi = 90°$). In this coordinate system, the angle between the proton velocity vector and the x direction is defined as the gyro-phase angle, θ, of a gyrating proton. The velocity vector can be written as $\mathbf{v} = v_\parallel\hat{z} + v_\perp\mathbf{e}_\perp$, where $\mathbf{e}_\perp = \cos\theta\hat{x} + \sin\theta\hat{y}$. Since for MSWs at quasi-perpendicular propagation the longitudinal component (i.e., E_x^w) of $\mathbf{E}^w$ is much larger (by several orders of magnitude, e.g., Gary et al. (2010)) than the transverse component, we only keep E_x^w in the subsequent derivation. In addition, the total magnetic field is $\mathbf{B} = (B_0 + B_z^w)\hat{z} \approx B_0\hat{z}$, since $|B_z^w| \ll B_0$. Assuming a sinusoidal wave of the form $E_x^w = \tilde{E}_x\cos\Phi$ (with the phase Φ to be defined later), the equations of motion in Eq. (6) may read

$$\dot{v}_\parallel = 0; \quad \dot{v}_\perp = \Omega_p c\frac{\tilde{E}_x}{B_0}\cos\Phi\cos\theta; \quad \text{and} \quad \dot{v}_\theta = -\Omega_p\left(v_\perp + c\frac{\tilde{E}_x}{B_0}\cos\Phi\sin\theta\right), \tag{7}$$

where the time derivatives are indicated by the over-dot notation. Equation for the gyro-phase is given by $\dot{\theta} = \dot{v}_\theta/v_\perp$. For all intents and purposes, $\dot{\theta} \approx -\Omega_p$ unless $v_\perp$ is really small and/or $\tilde{E}_x$ is really large.

The wave phase is given by

$$\Phi = \omega t - \int \mathbf{k}\cdot d\mathbf{r} = \omega t - \int k_x v_\perp\cos\theta dt. \tag{8}$$

If $\dot{\Phi} = 0$, then a test particle will see a constant phase for a longer-than-usual period of time. Therefore, the general condition for resonance may be expressed as

$$\cos\theta = \frac{\omega}{k_x v_\perp}. \tag{9}$$

Since $v_\perp > 0$, the solution to the above resonance condition is bracketed by $|\theta| \le \pi/2$, if $\omega/k_x > 0$ (i.e., forward propagating waves). If $v_\perp = \omega/k_x$, for example, a test particle sees a nearly constant wave phase near $\theta = 0$ and experiences a net acceleration. If, on the other hand, $v_\perp < |\omega/k_x|$, then the above condition will never be satisfied for any real value of θ. Nevertheless, these particles can still experience a net acceleration near $\theta = 0$ at which $\dot{\Phi}$ becomes minimum and thus the particle slows down in the wave reference frame.

The standard practice to proceed further is to recast the term involving $v_\perp$ in Φ using the Bessel function identity (e.g., J. Li et al., 2015). Assuming that $d\theta \approx -\Omega_p dt$ and $v_\perp$ is a slowly varying function of time, the wave phase can be written as

$$\Phi \approx \omega t + \Phi_0 + \xi \sin\theta, \tag{10}$$

where $\xi = k_x v_\perp/\Omega_p$. Following a procedure similar to J. Li et al. (2015) yields the approximate equations of motion

$$\dot{v}_\perp \approx \Omega_p c \frac{\tilde{E}_x}{B_0} \sum_{n=-\infty}^{\infty} \frac{n}{\xi} J_n(\xi) \cos\eta_n \tag{11}$$

and

$$\dot{v}_\theta \approx -\Omega_p \left(v_\perp + c\frac{\tilde{E}_x}{B_0} \sum_{n=-\infty}^{\infty} J_n'(\xi) \sin\eta_n \right), \tag{12}$$

where $\eta_n = \omega t + \Phi_0 + n\theta$. In this form, a wave that satisfies the usual cyclotron resonance condition $d\eta_n/dt = 0$ and thus $\omega = n\Omega_p$ contributes most to the net acceleration over multiple gyrations. Meanwhile, the Bessel function term in the $\dot{v}_\perp$ expression determines the efficiency of the acceleration. However, as will be shown, the assumption that $v_\perp$ is nearly constant in time has some important consequence under certain situations. We will discuss those in the next section.

It is straightforward to derive $D_{\perp\perp}$ from Eq. (11) by following the approach in, e.g., X. Li et al. (2015) and Bortnik et al. (2015). First, we consider a superposition of multiple monochromatic waves of the form

$$E_x^w(t) = \sum_{j=1}^{\infty} \tilde{E}_{x,j} \cos\Phi_j, \tag{13}$$

where $\Phi_j = \omega_j t - \int k_{x,j} dx$ and we are assuming $\omega_j/k_{x,j} > 0$. According to Parseval's theorem, the time average of the squared amplitude of E_x^w is given by

$$\left\langle (E_x^w)^2 \right\rangle = \frac{1}{2}\sum_{j=1}^{\infty} \tilde{E}_{x,j}^2 = \sum_{j=1}^{\infty} \frac{\Delta\omega}{\partial\omega_j/\partial k} |E_{\mathbf{k}}^x|_j^2, \tag{14}$$

where $|E_{\mathbf{k}}^x|^2$ is the power spectral density of E_x^w, $\langle \cdots \rangle = \tau^{-1}\int_0^\tau (\cdots) dt$, and $\tau = 2\pi/\Delta\omega$ is sufficiently large and multiples of $2\pi/\Omega_p$. With the expression for the wave superposition, Eq. (11) can be generalized to

$$\dot{v}_\perp = \Omega_p c \sum_{j=1}^{\infty} \frac{\tilde{E}_{x,j}}{B_0} \sum_{n=-\infty}^{\infty} \frac{n}{\xi_j} J_n(\xi_j) \cos\eta_{n,j}, \tag{15}$$

where $\eta_{n,j} = \omega_j t + \Phi_{0,j} + n\theta$ and $\xi_j = v_\perp k_{x,j}/\Omega_p$. The change of $v_\perp$ over the period is obtained from $\Delta v_\perp = \int_0^\tau \dot{v}_\perp dt$. Since we are integrating it along the unperturbed orbit, the only time-dependent term is $\cos\eta_{n,j}$. Substituting its time integral, $\int_0^\tau \cos\eta_{n,j} dt = \tau\cos\Phi_{0,j}\delta(\omega_j - n\Omega_p)$, into $\Delta v_\perp$ yields

$$\Delta v_\perp = \tau\Omega_p c \sum_{n=1}^{\infty} \frac{\tilde{E}_{x,n}}{B_0} \frac{n}{\xi_n} J_n(\xi_n) \cos\Phi_{0,n}. \tag{16}$$

Finally, from the definition of the diffusion coefficient $D_{\perp\perp} = \langle(\Delta v_\perp)^2\rangle/(2\tau)$ (where $\langle\cdots\rangle$ denotes average over $\Phi_{0,n}$) and using the Parseval's theorem, we get

$$D_{\perp\perp} = \pi\Omega_p^2 c^2 \sum_{n=1}^{\infty} \frac{|\tilde{E}^x_{\mathbf{k}}|^2}{B_0^2} \frac{1}{\partial\omega_n/\partial k} \frac{n^2}{\xi^2} J_n^2, \tag{17}$$

where the term inside the summation is evaluated at k such that $\omega(k) = n\Omega_p$. This expression is the same as the one from Eq. (2) with the assumptions that the electric field fluctuations are longitudinal, $\psi = 90°$, and the wave spectrum is one-sided.

3 Results

In this section, we use the formulations in the previous section to verify the QL diffusion due to MSWs of ψ approaching 90° and investigate in detail the test proton dynamics driven by MSWs at $\psi = 90°$. The background plasma parameters assumed throughout the paper are from Horne et al. (2000) where the background magnetic field magnitude is $B_0 = 256$ nT (or 2.56×10^{-3} gauss) and the total electron density is $n_0 = 18.97$ cm^{-3}. These parameters yield the ratio of the light to Alfvén speed $c/v_A = 234.6$, where the Alfvén speed is $v_A = B_0/\sqrt{4\pi m_p n_0}$. Note that this ratio is equal to the ratio of the proton plasma frequency to the proton cyclotron frequency, ω_p/Ω_p, where $\omega_p = \sqrt{4\pi n_0 e^2/m_p}$.

3.1 Quasilinear Diffusion Coefficient

In this subsection, we show the transition of $D_{\perp\perp}$ (the dominant diffusion coefficient for the parameters assumed here) as ψ approaches 90° and test whether $D_{\perp\perp}$ from QL theory is valid up to $\psi = 90°$ by comparing with the result from the TP method. As a broadband, incoherent wave spectrum needed as an input to Eq. (2), we adopt a Gaussian distribution for the magnetic field wave spectrum in wavenumber as follows:

$$W_B(k) = \frac{\varepsilon_B}{\sqrt{2\pi}\delta k} \exp\left(-\frac{(k-k_0)^2}{2\delta k^2}\right), \tag{18}$$

where k_0 is the wavenumber of the Gaussian peak, δk is the standard deviation, and ε_B is the total magnetic field wave energy density, $\varepsilon_B = \lim_{V\to\infty}\int_V |\mathbf{B}^w|^2/V d^3x$, where V is the volume. Since MSWs are composed of multiple harmonic modes, we choose a small value for $\delta k = 0.1\lambda_p^{-1}$ to represent a single harmonic mode of a narrow spectral width in wavenumber (see, e.g., Boardsen et al., 2018, Figure 2). (Here, $\lambda_p = c/\omega_p$ is the proton inertial length.) Correspondingly, the frequency span of the MSW spectral density is less than or about $0.5\Omega_p$. Since the wave frequency normalized to Ω_p is more intuitive to visualize MSWs, we also define $\omega_0 \equiv \omega(k_0)$ and use it interchangeably with k_0. We only consider $\omega_{\mathbf{k}} > 0$, which corresponds to forward propagating waves (provided $k > 0$). (Since the wave spectrum is symmetric, the case of $\omega_{\mathbf{k}} < 0$ is a mirror reflection of the result of the $\omega_{\mathbf{k}} > 0$ case with n replaced by $-n$.) The combined effect from multiple harmonic modes is a simple matter of adding up the individual contributions.

For TP computation, MSWs are described by superposition of $N_w = 101$ monochromatic waves with randomly chosen initial phases. The wavenumber of the ith monochromatic wave is determined by $k_i = k_0 + 2i\Delta k/(N_w - 1)$, where $i = 0, \pm1, \ldots, \pm(N_w - 1)/2$ and $\Delta k\lambda_p = 0.5$. The wave frequency and the root-mean-square amplitude of the magnetic field are determined from the cold plasma dispersion relation and from Eq. (18) according to Liu et al. (2012), respectively. For each batch of TP calculation, we trace a total of 1,000 test particles each of which is assigned randomly chosen initial location and randomly chosen initial gyro-phase. The diffusion coefficient, $D_{\perp\perp}$, is then obtained from the mean-square variation of the perpendicular velocity component, $\langle(\Delta v_\perp)^2\rangle$, following the method described by Liu et al. (2010, 2011).

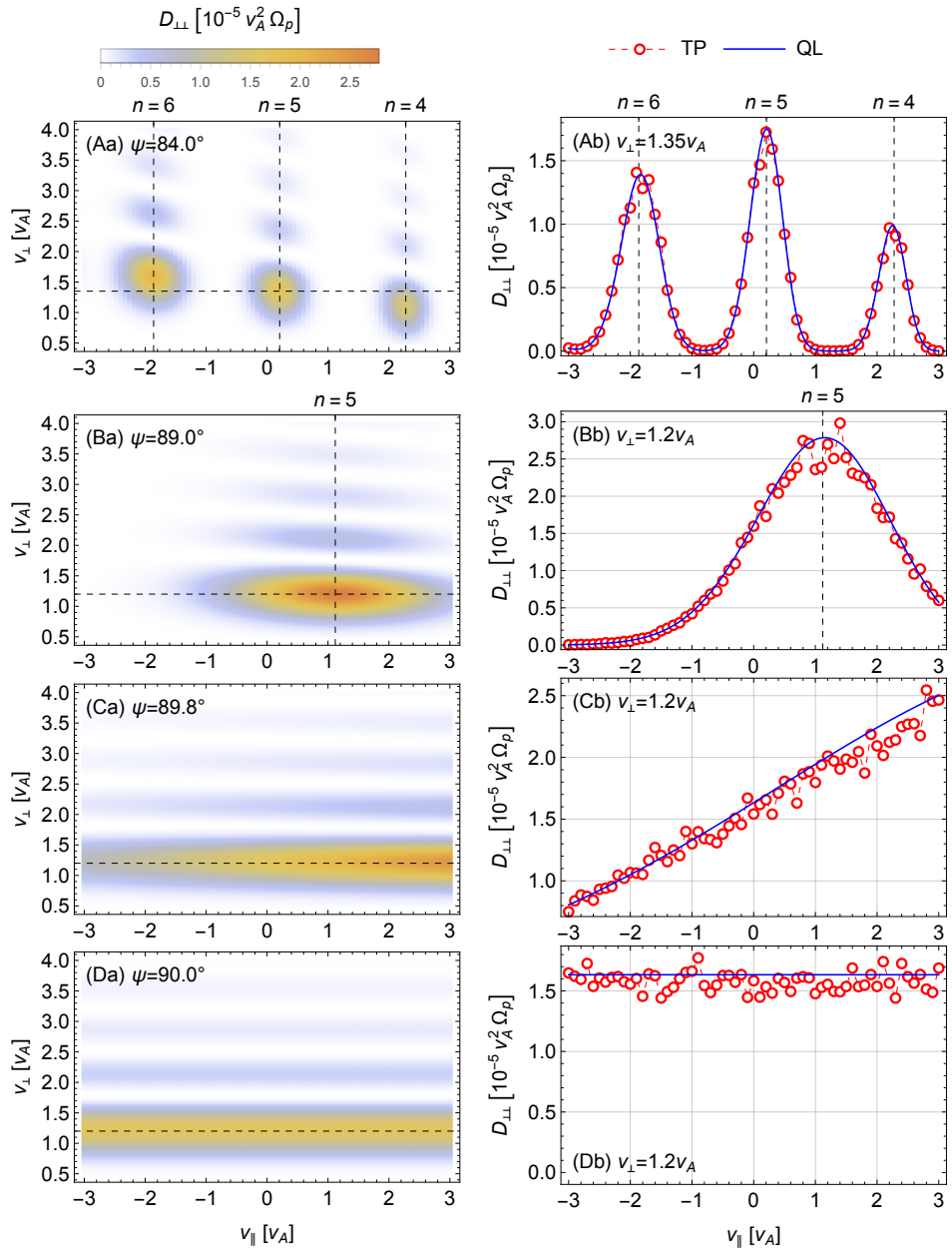

Figure 2. Comparison between $D_{\perp\perp}$'s from QL theory and TP computation for $\omega_0 = 5.1\Omega_p$ and $\varepsilon_B = 10^{-6}B_0^2$. From top to bottom the results correspond to $\psi = 84$, 89, 89.8, 90°, respectively. The panels in the left column display $D_{\perp\perp}$ from Eq. (2) as a function of $v_\parallel$ and $v_\perp$. The vertical dashed lines in the first two panels denote the resonant $v_\parallel$'s for the cyclotron resonance orders, $n = 4$, 5, and 6 with $\omega = \omega_0$. The horizontal dashed lines indicate the peak of $D_{\perp\perp}$ in $v_\perp$ for $n = 5$. The panels in the right column compare $D_{\perp\perp}$'s from QL theory (blue curves) and TP computation (red open circles). For each case of ψ, $v_\perp$ is fixed to a value indicated by the horizontal dashed line in the left column (also labeled in each panel).

In Figure 2, we fix $\omega_0 = 5.1\Omega_p$ and vary the wave normal angle: $\psi = 84$, 89, 89.8, and 90°. Then, the corresponding values of k_0 are 4.62, 5.12, 5.14, and 5.14, respectively. The panels in the left column (Column "a") display $D_{\perp\perp}$ obtained from Eq. (2). For $\psi = 84°$ (Figures 2Aa), there are three bright blobs of enhanced diffusion separated in $v_\parallel$, followed by smaller blobs with decreasing intensity at larger $v_\perp$. The resonant $v_\parallel$ of protons interacting with the dominant MSW is given by $v_\parallel = (\omega_0 - n\Omega_p)/(k_0 \cos\psi)$. Therefore, for $\psi = 84°$, the cyclotron resonance orders that yield $v_\parallel$ within the horizontal plot range are $n = 4$, 5, and 6; these are denoted in the figure with the vertical dashed lines. The subsequent, much weaker patches of diffusion in $v_\perp$ are due to the oscillating Bessel function present in Eq. (2). Since the argument, $\xi = k_\perp v_\perp/\Omega_p$, corresponding to the first peak of the Bessel function increases with an increasing Bessel function order (which is $\sim n$), there is almost a linear relation between n and $v_\perp$ at which the first peak of $D_{\perp\perp}$ occurs. When ψ increases to 89° (Figure 2Ba), the horizontal separation between the adjacent patches of enhanced diffusion increases and now all but the $n = 5$ contribution are beyond the horizontal plot scale. At the same time, the horizontal extent of the diffusion region associated with $n = 5$ also increases due to the Gaussian MSW spectrum about $k = k_0$, leading to an elongated patch. With $\psi = 89.8°$ (Figure 2Ca), the center of the $n = 5$ resonance lies outside the horizontal scale. Therefore, the diffusion shown in the figure is driven by the MSWs at the outskirts of the Gaussian distribution. Note that the dependence of $D_{\perp\perp}$ on $v_\parallel$ becomes weaker and weaker with an increasing ψ, to the point that $D_{\perp\perp}$ is independent of $v_\parallel$ at $\psi = 90°$ (Figure 2Da). At this point, the only resonant MSW is that of $\omega = 5\Omega_p$.

Since the TP method is computationally much more demanding, we only consider a one-dimensional slice of $D_{\perp\perp}$ at fixed $v_\perp$ for comparison. For the four wave normal angles considered, we choose initial $v_\perp = 1.35$, 1.2, 1.2, and $1.2v_A$, respectively, that correspond to the location of maximum $D_{\perp\perp}$ for the cyclotron resonance order $n = 5$ in the left column. (These are indicated with the horizontal dashed lines.) The panels in the right column of Figure 2 compare $D_{\perp\perp}$'s obtained from the two methods. Although there are some fluctuations of the points from the TP method at $\psi \approx 90°$, the agreement is generally very good. Particularly, as theory suggests, protons' $v_\parallel$ becomes irrelevant at $\psi = 90°$. This confirms that Eq. (2) is valid up to $\psi = 90°$.

In Figure 3, we carry out the same experiment with $\omega_0 = 5.5\Omega_p$. For better visualization of the main result, we accordingly select $\psi = 88$, 89, 89.5, and 89.8°. All other parameters are kept the same. In this case, since the dominant MSW has the half-integer harmonic frequency and the width of the wave spectrum is $\lesssim 0.5\Omega_p$ in frequency space, the diffusion rate at $v_\parallel = 0$ is minimum. At $\psi = 88°$, the $n = 5$ and 6 cyclotron resonance orders are still within the plot range. The QL diffusion coefficient agrees well with the one from the TP method. With an increasing ψ, those two resonance orders get further apart and the overall diffusion rates within the plot range decrease accordingly. At $\psi = 89.8°$, the QL diffusion rate is on the order of $10^{-10}v_A^2\Omega_p$ near $v_\parallel = 0$, whereas the TP method gives the rate on the order of $10^{-8}v_A^2\Omega_p$. This discrepancy can be most likely attributed to the statistical noise of the TP method, but may also indicate some physics missing in QL theory, such as nonlinear resonance broadening (Cai et al., 2020).

In Figure 4, we carry out a similar experiment with the 10th harmonic mode, $\omega_0 = 10\Omega_p$. All other parameters are kept the same, including $\varepsilon_B = 10^{-6}B_0$. The overall behavior of two-dimensional $D_{\perp\perp}$ is very similar to that shown in Figure 2, so it will not be shown. However, the comparison between QL theory and the TP method indicates that QL theory consistently overestimates the diffusion rate when the rate becomes larger than approximately $6\times10^{-5}v_A^2\Omega_p$. Since the maximum diffusion rate increases with increasing ψ (compare the global maximum of the blue curves), the discrepancy between the two methods gets larger as well. This is clearly the regime where the weak-wave assumption of QL theory starts to break down. Note that $D_{\perp\perp}$ in Eq. (2) is expressed in terms of $(E^w)^2$. So, even though ε_B is the same as the previous two cases, the ratio E^w/B^w

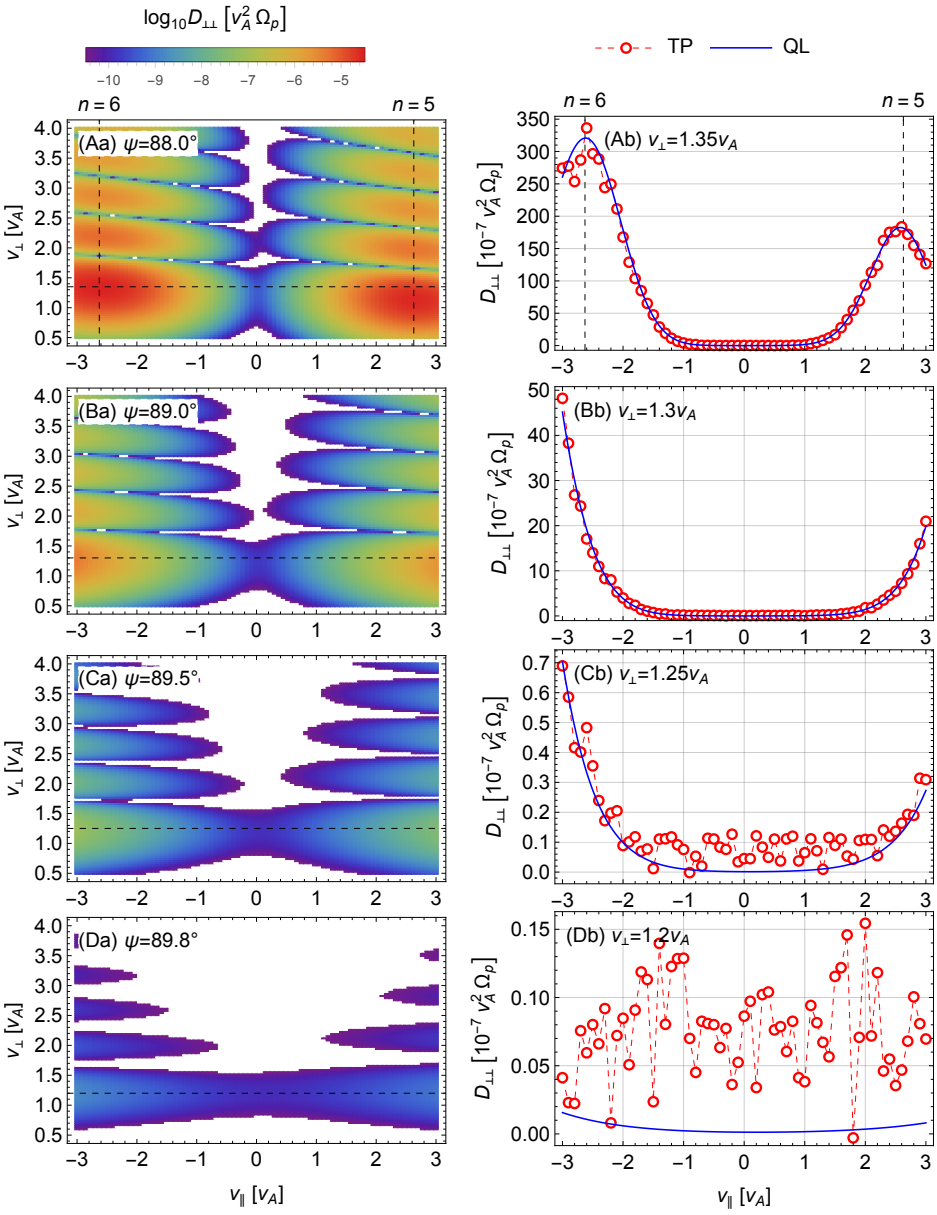

Figure 3. Same as Figure 2 except that $\omega_0 = 5.5\Omega_p$ and $\psi = 88$, 89, 89.5, and 89.8°. Also, $D_{\perp\perp}$ in the left column is shown in a logarithmic scale.

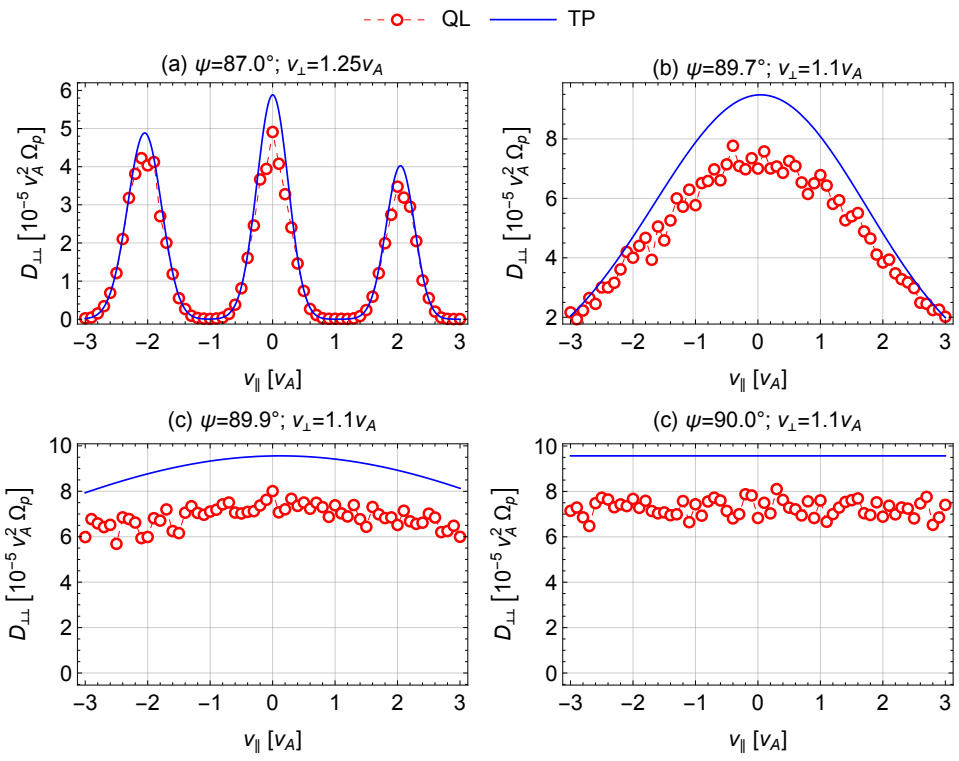

Figure 4. Comparison of $D_{\perp\perp}$ from QL theory (blue solid curves) with the one from the TP method (red open circles) for $\omega_0 = 10\Omega_p$ and $\psi = 87$, 89.5, 89.9, and 90°. The corresponding $v_\perp$ values are 1.25, 1.1, 1.1, and $1.1v_A$, respectively.

is an increasing function of ω. According to Boardsen et al. (2016, Figure 1), this ratio at $\omega = 10\Omega_p$ becomes twice as large as the ratio at $\omega = 5\Omega_p$, which means that $D_{\perp\perp}$ should increase roughly fourfold. In addition, the partial derivative, $|\partial\zeta_n/\partial k| \approx |\partial\omega/\partial k|$, in the denominator of Eq. (2) also decreases with increasing ψ, further contributing to the increase of $D_{\perp\perp}$ at $\psi \approx 90°$. As expected, lowering ε_B by one order of magnitude brings $D_{\perp\perp}$ to agreement with the one from the TP method (not shown).

3.2 Proton Dynamics with MSWs at $\psi = 90°$

Having proven that the diffusion coefficients of Eq. (2) are valid for MSWs of ψ up to 90°, we now turn our attention to understanding the proton dynamics in the presence of MSWs at $\psi = 90°$ and the ensuing scattering process. The premise of gyro-resonant interaction and the ensuing normal diffusion behavior is that a particle trajectory in momentum space exhibits a random walk-like behavior as a result of interactions with multiple incoherent waves described by a broadband spectrum. Every time a particle changes its momentum as a result of an interaction with one wave, its resonance condition also changes. This in turn enables the particle to resonate with other waves that meet the new resonance condition and this cycle repeats. The collective behavior of an ensemble of particles then amounts to a diffusive process. This line of thinking seems to break down once the wave normal angle of MSWs becomes 90°. Since according to QL theory the resonance condition is $\omega = n\Omega_p$, the same particle can resonate with the same wave regardless of its energy gain or loss after each interaction. Consequently, one may expect that the fate of each particle should be deterministic, rather than stochastic. To our knowledge such a situation has never been discussed before (at least in the magnetospheric context). Another matter we can shed some light on is whether the interaction of protons with MSWs at perpendicular propagation is resonant or non-resonant. Chen (2015) argued that the interaction in this context should be non-resonant because $v_\parallel$ becomes irrelevant and the parallel Doppler shift term disappears from the normal cyclotron resonance condition (thus leading to a simple frequency matching condition, $\omega = n\Omega_p$).

We first check how well the approximate formulations of Eqs. (7) and (11) do against the full Lorentz equation of Eq. (6). (The approximate equations are integrated along the unperturbed particle trajectory.) For this test, we launch test protons into a single MSW with magnetic field amplitude $\tilde{B}_z = 0.003B_0$ (a value sufficiently large to cause a large variation of $v_\perp$ in a relatively short time scale). All test protons initially have $v_\perp = 1.1v_A$ and $\theta = 0$. (Note that as we have shown earlier, $v_\parallel$ becomes irrelevant when $\psi = 90°$.) In Figures 5a–5b, we fix $\omega = 10\Omega_p$ (full integer harmonic mode) and choose the initial wave phases, $\Phi_0 = 0$ and π, respectively. Depending on the initial wave phase, the proton can gain or lose (perpendicular) energy. (The tracing time is normalized to the proton gyro-period, $T_p \equiv 2\pi/\Omega_p$.) Overall, both the electrostatic approximation of Eq. (7) and the Bessel sum approximation of Eq. (11) do a good job. Nevertheless, a noticeable deviation of behavior is clearly seen after $t \approx 30T_p$ in the solution of the Bessel sum approximation in Figure 5a, where the proton is supposed to decelerate. A similar behavior is also seen in Figure 5c for the case of $\Phi_0 = \pi/2$, where the Bessel sum approximation remains constant. It is worth noting that the $n = 10$ term in Eq. (11) sets the overall behavior (dashed magenta) and the other terms add minor corrections, such as the step-like increase and decrease of energy (blue curve). Since $\eta_{10}(t) = \Phi_0$ is constant, the $n = 10$ term contributes most to the net acceleration in Eq. (11) (see J. Li et al., 2015). Therefore, when $\Phi_0 = \pi/2$, the term $\cos\eta_{10}$ vanishes in Eq. (11) and the net acceleration becomes negligible. The vanishing acceleration in Figure 5a is for a different reason: $v_\perp \approx 1.4v_A$ is where the term $J_n(\xi)/\xi$ in Eq. (11) vanishes. In that sense, $J_n(\xi)/\xi$ acts as a weighting factor which determines the efficiency of acceleration. (Note that J_n is an oscillating function and can be negative.)

In Figures 5d–5f, we set $\Phi_0 = 0$, π, and $\pi/2$, respectively, with a fixed value of $\omega = 10.1\Omega_p$ (an off-integer harmonic mode). In this case, the overall peak-to-peak change

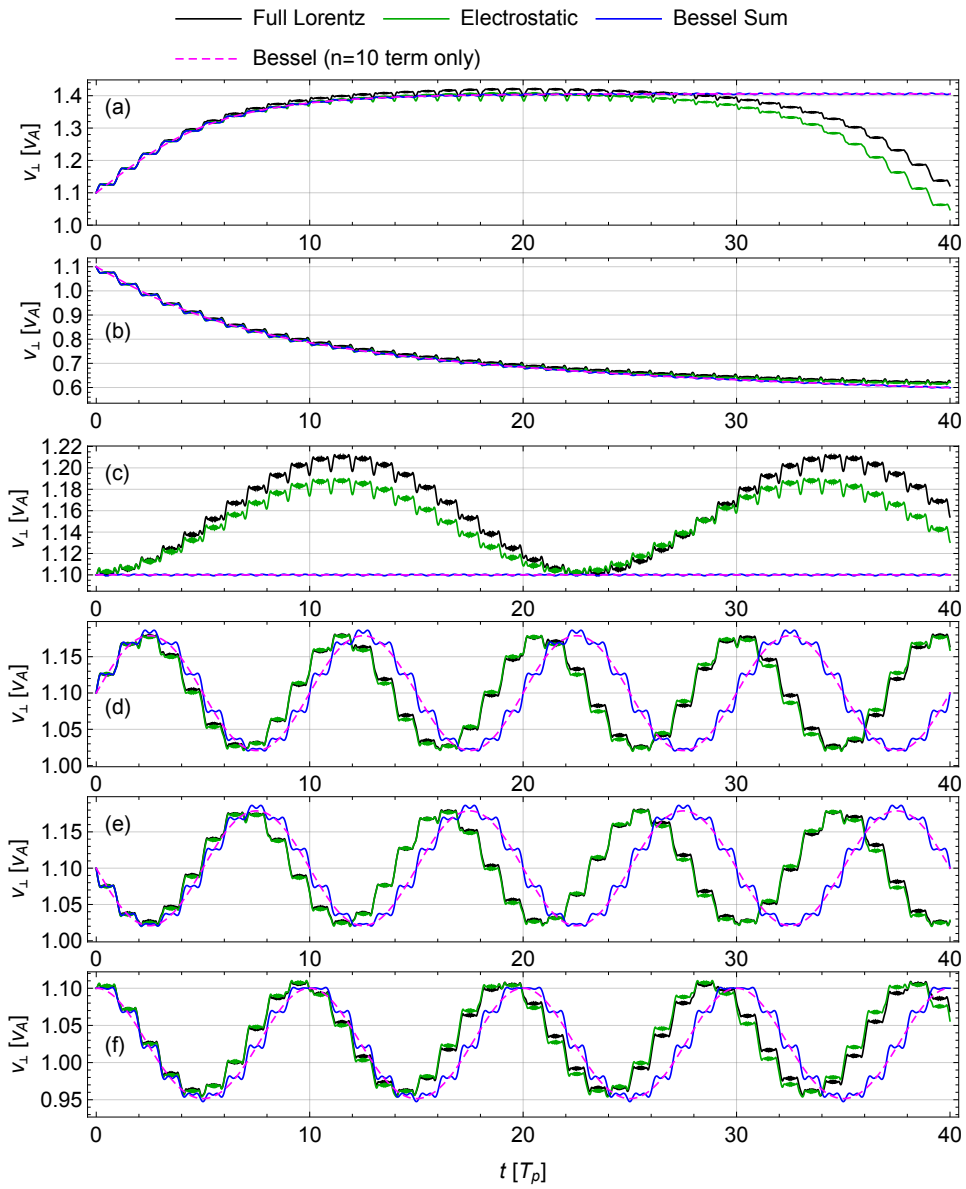

Figure 5. Comparison of test particle dynamics obtained from the full Lorentz equation of Eq. (6) (black), the electrostatic approximation of Eq. (7) (green), and the Bessel function approximation of Eq. (11). For the Bessel function approximation, the blue curves represent the calculation involving the sum over $n = 8, \ldots, 12$ in Eq. (11), whereas the dashed magenta curves represent the calculation involving only the $n = 10$ term. From top to bottom, the assumed parameters are as follows: (a) $\omega = 10\Omega_p$ and $\Phi_0 = 0$, (b) $\omega = 10\Omega_p$ and $\Phi_0 = \pi$, (c) $\omega = 10\Omega_p$ and $\Phi_0 = \pi/2$, (d) $\omega = 10.1\Omega_p$ and $\Phi_0 = 0$, (e) $\omega = 10.1\Omega_p$ and $\Phi_0 = \pi$, and (f) $\omega = 10.1\Omega_p$ and $\Phi_0 = \pi/2$. Other parameters common for all cases are: $\tilde{B}_z = 0.003B_0$, $v_\perp = 1.1v_A$, and $\theta = 0$. The tracing time is normalized to the proton gyro-period, T_p.

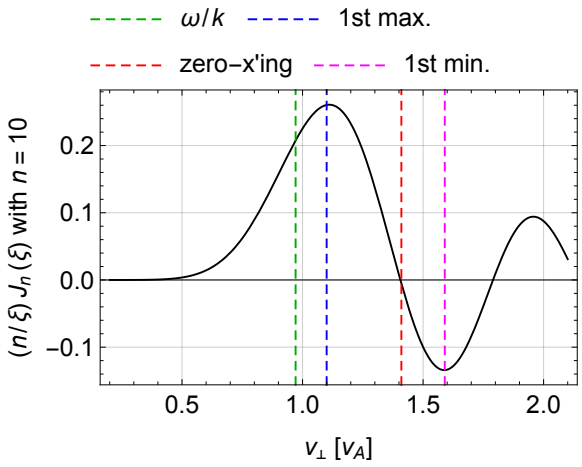

Figure 6. A plot of $(n/\xi)J_n(\xi)$ with $n = 10$ and $\omega = n\Omega_p$. The four vertical dashed lines from left denote ω/k_x, the first local maximum, the first zero crossing, and the first local minimum, respectively.

in $v_\perp$ is greatly reduced. Interestingly, the proton still exhibits a step-like variation in $v_\perp$ at every gyro-period. Both the electrostatic approximation of Eq. (7) and Bessel sum approximation of Eq. (11) do a good job tracking the oscillating $v_\perp$ variation for all three cases of Φ_0, although the phase of the latter approximation is apparently lagging behind. As before, the $n = 10$ term in Eq. (11) is sufficient to describe the overall behavior (compare the magenta and blue curves). Since $\eta_{10}(t) = \Phi_0 + 0.1t\Omega_p$ in this case, the periodicity of the energy variation is $10T_p$ in the Bessel sum approximation. (It is slightly smaller in the exact solution.)

The comparison in Figure 5 shows that the dynamics given by the Bessel sum approximation can deviate substantially from the full Lorentz solution for some combinations of initial parameters (such as the case in Figure 5c) and/or for long-term tracing. Recall that in simplifying the wave phase in Eq. (10) we have assumed that $v_\perp$ is constant over time. Although the time scale of the variation of $v_\perp$ is large compared with the gyro-period, its effect can accumulate in Eq. (8) to cause the deviations of the Bessel sum approximation shown in Figure 5. However, it can be also said that the Bessel sum approximation (a typically used technique in the gyro-averaging formulation) is reasonably good in capturing the overall behavior of the proton dynamics, particularly in the early phase. This is the reason why the QL theory formulation is applicable for waves at $\psi = 90°$. In addition, the formulation in the Bessel sum approximation can be useful to interpret full dynamic evolution of test protons obtained by solving the full Lorentz equation. As will be discussed below, one useful term is the weighting factor, $(n/\xi)J_n(\xi)$, which is plotted in Figure 6 versus $v_\perp$ with $n = 10$ and $\omega = n\Omega_p$.

One prominent feature in Figure 5 is the step-like change in $v_\perp$ which repeats at every gyro-period. To better understand how a proton interacts with a MSW at $\psi = 90°$, Figure 7 displays the time evolution of several parameters of a test proton. The initial parameters are $\omega = 10\Omega_p$, $\tilde{B}_z = 0.003B_0$, and $\Phi_0 = 0$ for the assumed MSW, and $v_\perp = 0.93v_A$ and $\theta = 0$ for the test proton. These parameters allow the test proton to see the maximum electric field at $\theta = 0$. Obviously, whenever there is a net increase in $v_\perp$, the proton sees a very slowly varying wave phase (Figure 7b), and thus the nearly constant E_x^w (Figure 7d). Quantitatively, the time derivative $d\Phi/dt$ becomes zero whenever Eq. (9) is satisfied, which can be solved for the gyro-phase, θ. If $v_\perp = \omega/k_x$, $d\Phi/dt$ becomes zero at $\theta = 0$ (green vertical dashed line). If $v_\perp < \omega/k_x$, there is no real so-

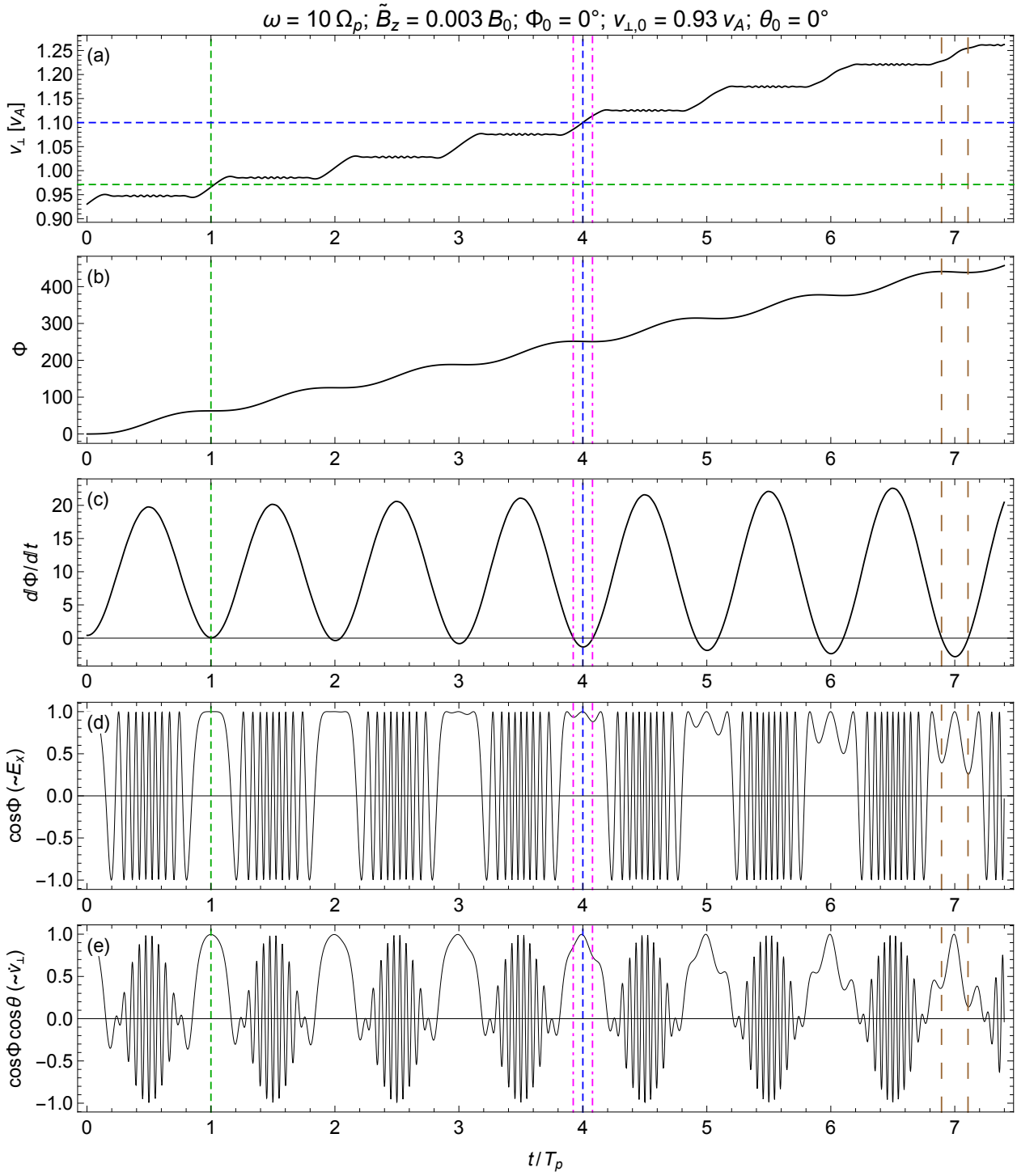

Figure 7. Evolution of a single proton parameters interacting with a MSW of $\omega = 10\Omega_p$. The initial parameters are $\tilde{B}_z = 0.003B_0$ and $\Phi_0 = 0$ for the MSW and $v_\perp = 0.93v_A$ and $\theta = 0$ for the test proton. From the top panel are (a) $v_\perp$, (b) Φ from Eq. (8), (c) $d\Phi/dt$, (d) $\cos\Phi$ (proportional to E_x^w seen by the particle), and (e) $\cos\Phi\cos\theta$ (proportional to $\dot{v}_\perp$ in Eq. (7)) as a function of time normalized to the proton gyro-period, T_p. The horizontal dashed lines in panel (a) are drawn at $v_\perp = \omega/k_x$ (green) and $1.1v_A$ (blue), respectively. The vertical magenta and brown dashed lines indicate the $\pm 28°$ and $\pm 38.4°$ gyro-phase offsets respectively about $t/T_p = 4$ and 7.

lution for θ (see the time $t = 0$) and if $v_\perp > \omega/k_x$, then there are two solutions for θ. For example, at $v_\perp \approx 1.1v_A$ the two solutions of Eq. (9) are $\theta \approx \pm 28°$ (indicated by the vertical magenta lines). Since in Eq. (7) the term, $\cos\Phi\cos\theta$, represents the acceleration, the area under the curve in Figure 7e indicates the net change in $v_\perp$ over that time period. As a result, the test proton experiences a net change in $v_\perp$ for a brief moment whenever its gyro-phase passes through zero, whereas the net change in $v_\perp$ averages to zero for other regions of the gyro-phase. This net change becomes largest at $v_\perp$ where the first peak of $J_n(\xi)/\xi$ occurs. For $\omega = 10\Omega_p$, this value is about $1.1v_A$, indicated with the blue dashed lines both in Figures 6 and 7. If $v_\perp$ increases beyond this limit, the gyro-phases satisfying Eq. (9) deviate further from zero, where the electric field seen by the proton is further reduced and so is the net acceleration; see for example the vertical brown dashed lines in Figure 7. It is at $v_\perp \approx 1.41v_A$ (equivalently $\xi \approx 14.5$) at which $J_{10}(\xi)/\xi = 0$ and the net acceleration becomes approximately zero. On the other hand, if $v_\perp < \omega/k_x$, $d\Phi/dt$ is always positive and there is no real solution for θ that satisfies Eq. (9). Nevertheless, the particle slows down when it passes through $\theta = 0$ and depending on Φ_0 it can still experience a net change in $v_\perp$. Since $J_n(\xi)/\xi$ approaches zero (see Figure 6), however, the efficiency of acceleration rapidly diminishes with decreasing $v_\perp$.

Figure 8 schematically depicts the wave-particle interaction for the case of $v_\perp > \omega/k_x$ and $\Phi_0 = \theta = 0$. The particle sees the maximum value of E_x at locations 1, 3, and 5. On the other hand, the condition of Eq. (9) is satisfied at locations 2 and 4. Since the x component of the proton's velocity is $v_x = v_\perp\cos\theta$, the wave phase velocity, ω/k_x, becomes the same as v_x at locations, 2 and 4. Therefore, up to point 2, the wave catches up the proton because $v_x < \omega/k_x$ and its location happens to be behind the crest of E_x for this test setup, as shown in Figure 8c. Between points 2 and 4, the proton moves faster in the x direction than the wave does because $v_x > \omega/k_x$ during this interval. As a result, the proton moves to the other side of the crest, as shown in Figure 8c. Past this point, $v_x < \omega/k_x$ again and the proton is passed by the wave for multiple wavelengths until the gyro-phase returns to point 1 in Figure 8b at which the cycle repeats.

The dynamics of two sample protons interacting with off-integer harmonic MSWs of the frequency $\omega/\Omega_p = 10.1$ and 10.5, respectively, are shown in Figure 9. For both cases, the initial parameters are tuned so that at $t = 0$ the test protons see the maximum electric field. Interestingly, the protons experience a step-like increase/decrease in energy as well, even though they are supposed to be non-resonant with the off-integer harmonic waves, according to the usual cyclotron resonance condition. Recall that for the integer harmonic case, the proton sees more or less the same wave phase every time its gyro-phase passes through zero (Figure 7d). However, if the wave frequency has a fractional part (as are the test cases here), the wave phase that the proton sees at $\theta = 0$ drifts over time and gets out of sync with the gyro-phase. Because of that, the proton does not gain or lose energy consecutively as it does when it interacts with an integer harmonic MSW (see Figure 5). The de-tuning between the wave phase and the gyro-phase is responsible for the longer scale periodicity in the energy variation discussed in Figures 5d–5f. An extreme case is when the fractional part becomes half the proton cyclotron frequency, as shown in Figures 9c and 9d. In this case, the proton sees an alternating wave phase.

Before concluding this subsection, we examine the effect of wave superposition on the proton dynamics. In this test, five monochromatic MSWs of the identical amplitude are used with randomly chosen initial phases. (In comparison, $N_w = 101$ monochromatic MSWs have been used to obtain $D_{\perp\perp}$ previously.) The total root-mean-square amplitude is $0.001B_0$. In Figure 10a, the frequencies of the monochromatic waves are ω/Ω_p = 9.9, 9.95, 10, 10.05, 10.1, respectively, representing a narrowband spectrum centered at the 10th harmonic. Eight test protons are traced in this wave field, with the same initial $v_\perp = 1.1v_A$ but randomly chosen gyro-phase and initial location. Some particles

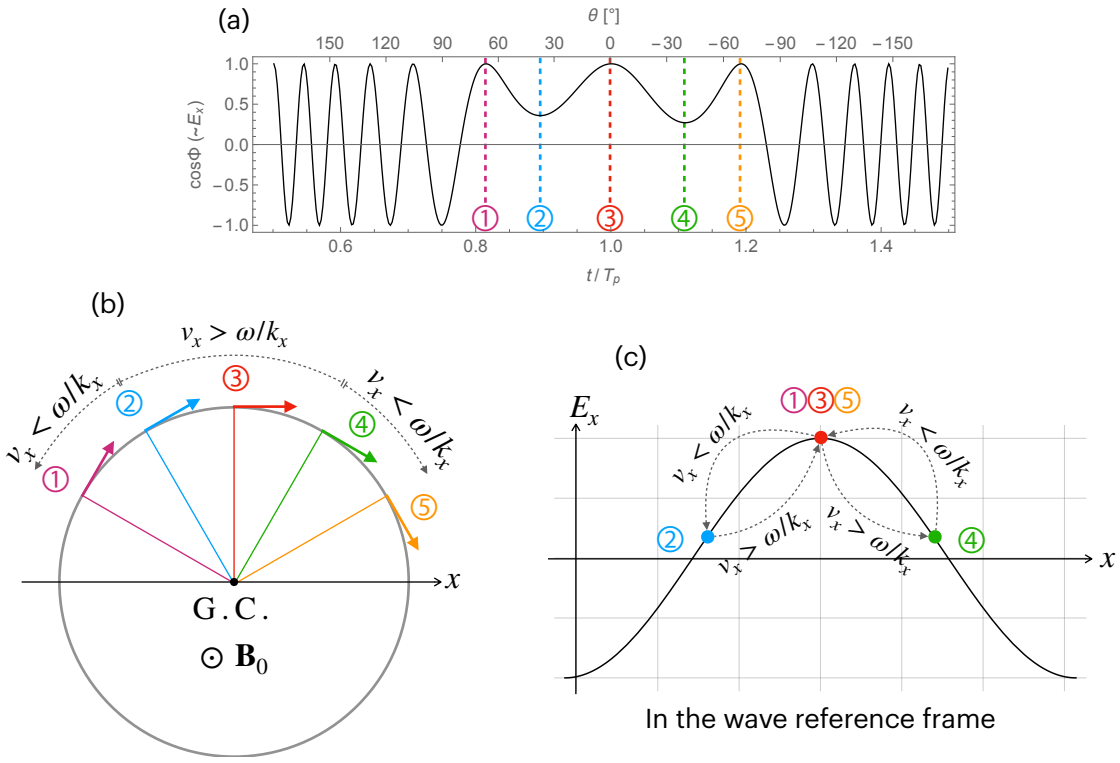

Figure 8. Schematic illustration of the wave-particle interaction occurring at the gyro-phase where an acceleration occurs in the case of $v_\perp > \omega/k_x$ and $\Phi_0 = 0$. (a) The electric field, E_x, seen by the test proton. The interval marked by the circled numbers, 1–5, is where the net acceleration becomes positive. The bottom tick labels denote the time normalized to the proton gyro-period and the top tick labels denote the gyro-phase angle, θ. (b) Proton locations relative to the guiding center and the velocity vectors of the test proton at the times indicated by the circled numbers in panel (a). The magnitude of the x component of the velocity, $v_x = v_\perp \cos\theta$, relative to the wave phase speed, ω/k_x, is denoted in each interval. The background magnetic field, $\mathbf{B}_0$, is coming out of the plane. (c) Proton trajectory in the wave reference frame during the time period, 1–5, in panel (a). The gray dotted arrows indicate the directions of particle movement during the intermediate intervals, along with v_x to ω/k_x.

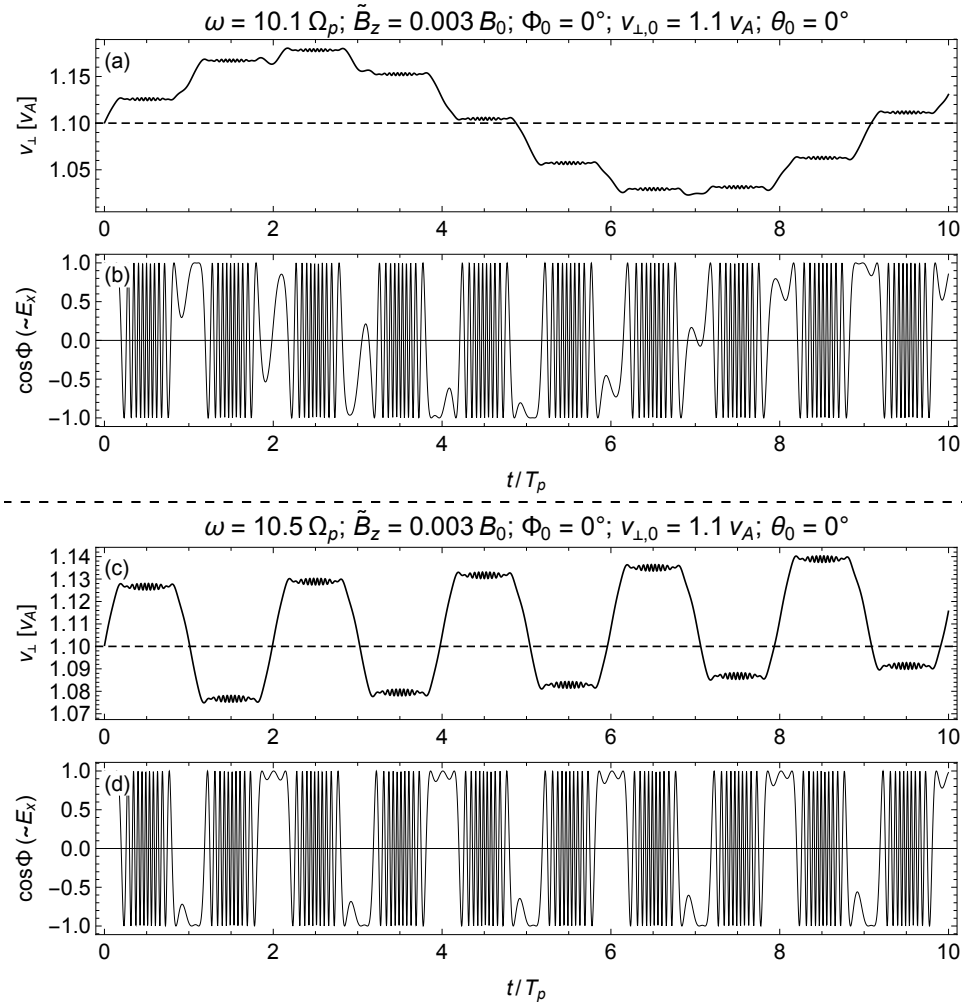

Figure 9. Dynamic evolutions of (a and c) $v_\perp$ and (b and d) $\cos\Phi$ of two test protons interacting with off-integer harmonic MSWs. The initial parameters common to both cases are: $v_\perp = 1.1v_A$, $\theta = 0$, $\Phi_0 = 0$, and $\tilde{B}_z = 0.003B_0$. (a–b) Result for $\omega = 10.1\Omega_p$. (c–d) Result for $\omega = 10.5\Omega_p$.

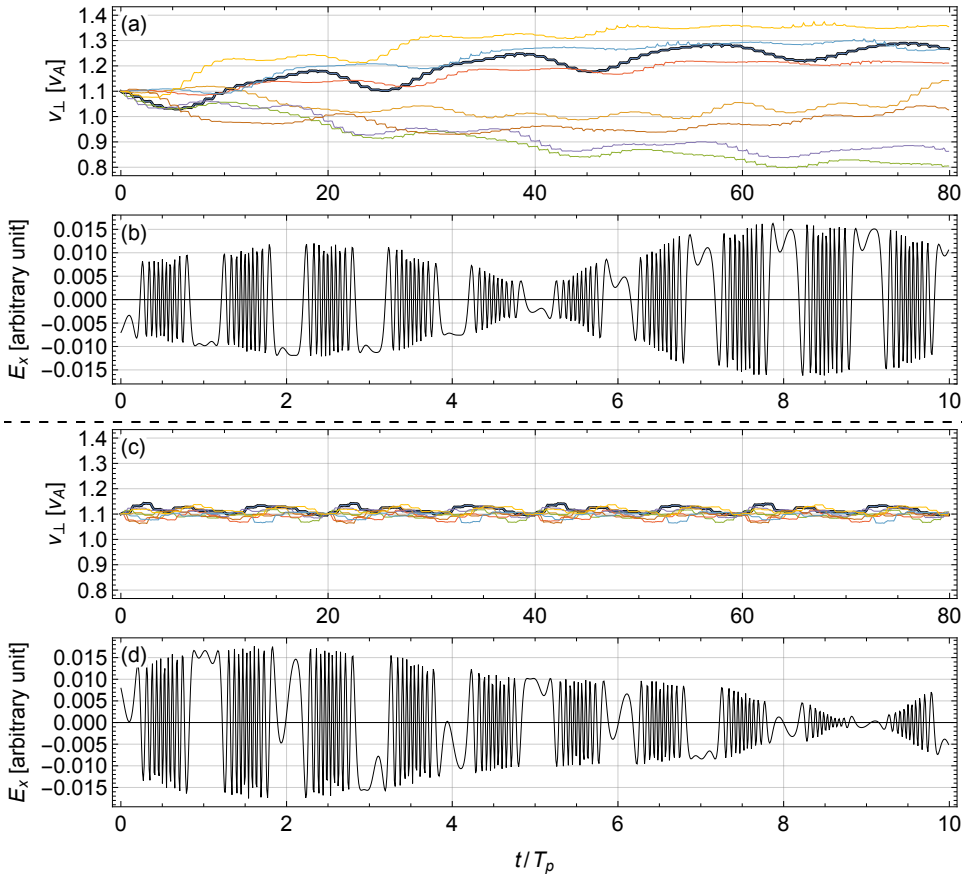

Figure 10. Effect of wave superposition on the test proton scattering. Five monochromatic MSWs of the identical amplitude are used with randomly chosen initial phases. The total root-mean-square amplitude is $0.001B_0$. In panels a and b, the wave frequencies are $\omega/\Omega_p = 9.9$, 9.95, 10, 10.05, 10.1, respectively, representing a narrowband spectrum centered at the 10th harmonic. In panels c and d, the wave frequencies are $\omega/\Omega_p = 10.1$, 10.15, 10.2, 10.25, 10.3, respectively, representing an off-integer harmonic, narrowband spectrum. Panels a and c display the $v_\perp$ evolutions of eight test protons whose initial gyro-phase and location are chosen randomly. Panels b and d each display the electric field for the first ten gyro-periods seen by one test proton indicated by a thick black curve in the $v_\perp$ plot. Time is normalized by the proton gyro-period, T_p.

get energized while others lose energy, but the main difference from the monochromatic case in Figure 5 is that the $v_\perp$ variation exhibits a random walk-like behavior, similar to cyclotron resonance shown in Tao et al. (2011) and Liu et al. (2012). In contrast, a narrowband spectrum centered at an off-integer harmonic frequency is assumed in Figure 10c, where the frequencies are $\omega/\Omega_p = 10.1$, 10.15, 10.2, 10.25, 10.3, respectively. Even with the slightly off-centered spectrum, the maximum deviation in $v_\perp$ is only a fraction of that for the integer harmonic case. Figures 10b and 10d display the electric field seen by one proton selected from each test group. In both cases, the direction of the electric field seen by the proton at $\theta \approx 0$ changes more quickly as a result of superposition, compared with the monochromatic case (cf. Figure 7d). Furthermore, in Figure 10d, the change in the electric field direction is more frequent in that the direction of E_x that the particle sees at $\theta \approx 0$ flips roughly at every other gyro-period. As a result, only minor deviation in $v_\perp$ ensues when there is no integer harmonic mode in the spectrum. This simple test suggests that although low in amplitude, the presence of off-integer harmonic MSWs in the vicinity of the integer harmonic mode (see, e.g., Boardsen et al., 2018, Figure 2) is important to make the scattering behavior stochastic.

4 Summary and Discussion

Calculation of the QL diffusion coefficients typically avoids waves of $\psi \approx 90°$ by using a truncated Gaussian model with $\tan\psi$ as its independent variable, even though there is no restriction on the wave normal angle range in the QL formulation of, e.g., Kennel and Engelmann (1966). Many cases in the inner magnetosphere may be well within this constraint because major plasma waves typically have a distribution in wave normal angle far away from 90°. There are, however, wave modes such as MSWs, that can exhibit the largest growth rate and amplitude at $\psi \approx 90°$ and thus lie outside the domain of the presumed model. Particularly, the effect of MSWs at quasi-perpendicular propagation can be substantial for ring current proton scattering because the high-order cyclotron resonances play a dominant role.

In the present study, we have confirmed the validity of the QL diffusion coefficients driven by MSWs of ψ up to 90° in two different ways: comparison with the diffusion coefficients from the test-particle method with varying ψ and the direct derivation of the diffusion coefficient from the test-particle dynamic equations at $\psi = 90°$ assuming an electrostatic approximation. In addition, we have investigated in detail the dynamics of protons interacting with MSWs at $\psi = 90°$. Although in QL theory the resonance condition is $\omega = n\Omega_p$ for a harmonic order n, the presence of off-integer harmonic MSWs in the vicinity of the integer harmonic mode (see, e.g., Boardsen et al., 2018, Figure 2) is important to make the proton scattering process stochastic.

One natural question to ask is how important it is to include MSWs with $\psi \gtrsim 89.5°$ on the proton dynamics in the inner magnetosphere, such as suprathermal proton heating (Teng et al., 2019). We cannot answer this question in its fullest extent in the present study, but if previous studies are any indication, the importance of MSWs at quasi-perpendicular propagation may have be shown in Fu and Ge (2021). Fu and Ge (2021) investigated the ring current proton scattering by MSWs having a broadband spectrum confined near the magnetic equator in a dipole magnetic field using the test-particle approach. Figure 5 therein clearly indicates that the energy diffusion rate at $\psi = 89.9°$ is maintained as strong (if not stronger) as the rate at $\psi = 89°$. Therefore, since both the observation (Boardsen et al., 2018) and the simulation (Min et al., 2020) suggested substantial wave power at quasi-perpendicular propagation, the QL diffusion using the truncated Gaussian model will underestimate the ring current proton scattering in a non-negligible way.

As a final point, some studies attribute very low-energy proton heating frequently observed in the inner magnetosphere to the proton scattering by MSWs that sometimes accompany the heating. As far as the QL diffusion is concerned, Eq. (17) together with

Figure 6 indicates that $D_{\perp\perp}$ tends to zero rapidly as $v_\perp$ decreases below approximately the perpendicular wave phase speed. Although not shown here, we have confirmed from the test-particle calculation that the proton scattering becomes negligible at such low energy. The inefficiency of MSW-driven proton scattering at low energy has also been suggested in previous studies (Curtis, 1985; Horne et al., 2000). Nevertheless, kinetic simulations suggested that the low-energy protons experience heating in the perpendicular direction with respect to the background magnetic field. So, if the heating is related to MSWs, it should be some kind of non-resonant process beyond the QL regime that operates most effectively on low-energy protons (e.g., Artemyev et al., 2017). Revealing such a process is highly relevant to the role of MSWs on thermal protons in the inner magnetosphere and thus deserves further investigation.

Acknowledgments

This work was supported by the National Research Foundation of Korea (NRF) grant funded by the Korea government (MSIT) (No. 2020R1C1C1009996) and by research fund of Chungnam National University. All the data used to make the figures in the text can be obtained using the equations and the parameters in Sections 2 and 3.

References

Albert, J. M. (2005, March). Evaluation of quasi-linear diffusion coefficients for whistler mode waves in a plasma with arbitrary density ratio. *Journal of Geophysical Research (Space Physics)*, *110*(A3), A03218. doi: 10.1029/2004JA010844

Albert, J. M. (2007, December). Simple approximations of quasi-linear diffusion coefficients. *Journal of Geophysical Research (Space Physics)*, *112*(A12), A12202. doi: 10.1029/2007JA012551

Artemyev, A. V., Mourenas, D., Agapitov, O. V., & Blum, L. (2017, February). Transverse eV ion heating by random electric field fluctuations in the plasmasphere. *Physics of Plasmas*, *24*(2), 022903. doi: 10.1063/1.4976713

Birdsall, C. K., & Langdon, A. B. (2004). *Plasma Physics via Computer Simulation*. Taylor & Francis. Retrieved from `https://books.google.com/books?id=S2lqgDTm6a4C`

Boardsen, S. A., Hospodarsky, G. B., Kletzing, C. A., Engebretson, M. J., Pfaff, R. F., Wygant, J. R., ... De Pascuale, S. (2016, April). Survey of the frequency dependent latitudinal distribution of the fast magnetosonic wave mode from Van Allen Probes Electric and Magnetic Field Instrument and Integrated Science waveform receiver plasma wave analysis. *Journal of Geophysical Research (Space Physics)*, *121*, 2902-2921. doi: 10.1002/2015JA021844

Boardsen, S. A., Hospodarsky, G. B., Min, K., Averkamp, T. F., Bounds, S. R., Kletzing, C. A., & Pfaff, R. F. (2018, August). Determining the Wave Vector Direction of Equatorial Fast Magnetosonic Waves. *Geophys. Res. Lett.*, *45*, 7951-7959. doi: 10.1029/2018GL078695

Bortnik, J., Thorne, R. M., Ni, B., & Li, J. (2015, March). Analytical approximation of transit time scattering due to magnetosonic waves. *Geophys. Res. Lett.*, *42*, 1318-1325. doi: 10.1002/2014GL062710

Cai, B., Wu, Y., & Tao, X. (2020, June). Effects of Nonlinear Resonance Broadening on Interactions Between Electrons and Whistler Mode Waves. *Geophys. Res. Lett.*, *47*(11), e87991. doi: 10.1029/2020GL087991

Chen, L. (2015, June). Wave normal angle and frequency characteristics of magnetosonic wave linear instability. *Geophys. Res. Lett.*, *42*, 4709-4715. doi: 10.1002/2015GL064237

Curtis, S. A. (1985, February). Equatorial trapped plasmasphere ion distributions and transverse stochastic acceleration. *J. Geophys. Res.*, *90*(A2), 1765-1770.

561 doi: 10.1029/JA090iA02p01765
562 Drozdov, A. Y., Usanova, M. E., Hudson, M. K., Allison, H. J., & Shprits, Y. Y.
563 (2020, September). The Role of Hiss, Chorus, and EMIC Waves in the
564 Modeling of the Dynamics of the Multi-MeV Radiation Belt Electrons.
565 *Journal of Geophysical Research (Space Physics)*, *125*(9), e28282. doi:
566 10.1029/2020JA028282
567 Fu, S., & Ge, Y. (2021, feb). Acceleration of Ring Current Protons Driven by
568 Magnetosonic Waves: Comparisons of Test Particle Simulations with Quasi-
569 linear Calculations. *The Astrophysical Journal*, *908*(2), 203. Retrieved from
570 `https://doi.org/10.3847/1538-4357/abd2b3` doi: 10.3847/1538-4357/
571 abd2b3
572 Fu, S., Ni, B., Li, J., Zhou, C., Gu, X., Huang, S., ... Cao, X. (2016, September).
573 Interactions between magnetosonic waves and ring current protons: Gyroav-
574 eraged test particle simulations. *Journal of Geophysical Research (Space*
575 *Physics)*, *121*(9), 8537-8553. doi: 10.1002/2016JA023117
576 Gary, S. P., Liu, K., Winske, D., & Denton, R. E. (2010, December). Ion Bern-
577 stein instability in the terrestrial magnetosphere: Linear dispersion theory.
578 *Journal of Geophysical Research (Space Physics)*, *115*(A12), A12209. doi:
579 10.1029/2010JA015965
580 Glauert, S. A., & Horne, R. B. (2005, April). Calculation of pitch angle and energy
581 diffusion coefficients with the PADIE code. *Journal of Geophysical Research*
582 *(Space Physics)*, *110*(A4), A04206. doi: 10.1029/2004JA010851
583 Horne, R. B., Thorne, R. M., Glauert, S. A., Meredith, N. P., Pokhotelov, D., &
584 Santolík, O. (2007, September). Electron acceleration in the Van Allen radia-
585 tion belts by fast magnetosonic waves. *Geophys. Res. Lett.*, *34*, L17107. doi:
586 10.1029/2007GL030267
587 Horne, R. B., Wheeler, G. V., & Alleyne, H. S. C. K. (2000, December). Proton and
588 electron heating by radially propagating fast magnetosonic waves. *J. Geophys.*
589 *Res.*, *105*, 27597-27610. doi: 10.1029/2000JA000018
590 Kennel, C. F., & Engelmann, F. (1966, December). Velocity Space Diffusion from
591 Weak Plasma Turbulence in a Magnetic Field. *Physics of Fluids*, *9*(12), 2377-
592 2388. doi: 10.1063/1.1761629
593 Lei, M., Xie, L., Li, J., Pu, Z., Fu, S., Ni, B., ... Li, W. (2017, December). The
594 Radiation Belt Electron Scattering by Magnetosonic Wave: Dependence on
595 Key Parameters. *Journal of Geophysical Research (Space Physics)*, *122*, 12.
596 doi: 10.1002/2016JA023801
597 Li, J., Bortnik, J., Xie, L., Pu, Z., Chen, L., Ni, B., ... Guo, R. (2015, May).
598 Comparison of formulas for resonant interactions between energetic electrons
599 and oblique whistler-mode waves. *Physics of Plasmas*, *22*(5), 052902. doi:
600 10.1063/1.4914852
601 Li, X., Tao, X., Lu, Q., & Dai, L. (2015, November). Bounce resonance diffusion co-
602 efficients for spatially confined waves. *Geophys. Res. Lett.*, *42*, 9591-9599. doi:
603 10.1002/2015GL066324
604 Liu, K., Gary, S. P., & Winske, D. (2011, July). Excitation of magnetosonic waves
605 in the terrestrial magnetosphere: Particle-in-cell simulations. *Journal of Geo-*
606 *physical Research (Space Physics)*, *116*, A07212. doi: 10.1029/2010JA016372
607 Liu, K., Lemons, D. S., Winske, D., & Gary, S. P. (2010, April). Relativistic electron
608 scattering by electromagnetic ion cyclotron fluctuations: Test particle simula-
609 tions. *Journal of Geophysical Research (Space Physics)*, *115*(A4), A04204. doi:
610 10.1029/2009JA014807
611 Liu, K., Winske, D., Gary, S. P., & Reeves, G. D. (2012, June). Relativistic elec-
612 tron scattering by large amplitude electromagnetic ion cyclotron waves: The
613 role of phase bunching and trapping. *Journal of Geophysical Research (Space*
614 *Physics)*, *117*(A6), A06218. doi: 10.1029/2011JA017476
615 Lyons, L. R. (1974, December). Pitch angle and energy diffusion coefficients from

resonant interactions with ion-cyclotron and whistler waves. *Journal of Plasma Physics*, *12*(3), 417-432. doi: 10.1017/S002237780002537X

Ma, Q., Li, W., Thorne, R. M., Ni, B., Kletzing, C. A., Kurth, W. S., ... Angelopoulos, V. (2015, February). Modeling inward diffusion and slow decay of energetic electrons in the Earth's outer radiation belt. *Geophys. Res. Lett.*, *42*(4), 987-995. doi: 10.1002/2014GL062977

Ma, Q., Li, W., Yue, C., Thorne, R. M., Bortnik, J., Kletzing, C. A., ... Spence, H. E. (2019, June). Ion Heating by Electromagnetic Ion Cyclotron Waves and Magnetosonic Waves in the Earth's Inner Magnetosphere. *Geophys. Res. Lett.*, *46*(12), 6258-6267. doi: 10.1029/2019GL083513

Min, K., Liu, K., Denton, R. E., Němec, F., Boardsen, S. A., & Miyoshi, Y. (2020, October). Two-Dimensional Hybrid Particle-in-Cell Simulations of Magnetosonic Waves in the Dipole Magnetic Field: On a Constant L-Shell. *Journal of Geophysical Research (Space Physics)*, *125*(10), e28414. doi: 10.1029/2020JA028414

Mourenas, D., Artemyev, A. V., Agapitov, O. V., & Krasnoselskikh, V. (2013, June). Analytical estimates of electron quasi-linear diffusion by fast magnetosonic waves. *Journal of Geophysical Research (Space Physics)*, *118*, 3096-3112. doi: 10.1002/jgra.50349

Ni, B., Hua, M., Zhou, R., Yi, J., & Fu, S. (2017, April). Competition between outer zone electron scattering by plasmaspheric hiss and magnetosonic waves. *Geophys. Res. Lett.*, *44*, 3465-3474. doi: 10.1002/2017GL072989

Schulz, M., & Lanzerotti, L. J. (1974, January). Particle Diffusion in the Radiation Belts. *Physics and Chemistry in Space*, *7*. doi: 10.1007/978-3-642-65675-0

Summers, D. (2005, August). Quasi-linear diffusion coefficients for field-aligned electromagnetic waves with applications to the magnetosphere. *Journal of Geophysical Research (Space Physics)*, *110*(A8), A08213. doi: 10.1029/2005JA011159

Tao, X., Bortnik, J., Albert, J. M., Liu, K., & Thorne, R. M. (2011, March). Comparison of quasilinear diffusion coefficients for parallel propagating whistler mode waves with test particle simulations. *Geophys. Res. Lett.*, *38*(6), L06105. doi: 10.1029/2011GL046787

Teng, S., Li, W., Tao, X., Ma, Q., Wu, Y., Capannolo, L., ... Gan, L. (2019, December). Generation and Characteristics of Unusual High Frequency EMIC Waves. *Geophys. Res. Lett.*, *46*(24), 14,230-14,238. doi: 10.1029/2019GL085220

Thorne, R. M. (2010, November). Radiation belt dynamics: The importance of wave-particle interactions. *Geophys. Res. Lett.*, *37*(22), L22107. doi: 10.1029/2010GL044990

Thorne, R. M., Li, W., Ni, B., Ma, Q., Bortnik, J., Chen, L., ... Kanekal, S. G. (2013, December). Rapid local acceleration of relativistic radiation-belt electrons by magnetospheric chorus. *Nature*, *504*(7480), 411-414. doi: 10.1038/nature12889

Xiao, F., Yang, C., Su, Z., Zhou, Q., He, Z., He, Y., ... Blake, J. B. (2015, October). Wave-driven butterfly distribution of Van Allen belt relativistic electrons. *Nature Communications*, *6*, 8590. doi: 10.1038/ncomms9590

Xiao, F., Zong, Q., Wang, Y., He, Z., Su, Z., Yang, C., & Zhou, Q. (2014, June). Generation of proton aurora by magnetosonic waves. *Scientific Reports*, *4*, 5190. doi: 10.1038/srep05190